Since January 2020 Elsevier has created a COVID-19 resource centre with free information in English and Mandarin on the novel coronavirus COVID-19. The COVID-19 resource centre is hosted on Elsevier Connect, the company's public news and information website.

European Journal of Medicinal Chemistry 167 (2019) 472–484

Contents lists available at ScienceDirect

European Journal of Medicinal Chemistry

journal homepage: http://www.elsevier.com/locate/ejmech

Research paper

Chemical synthesis, crystal structure, versatile evaluation of their biological activities and molecular simulations of novel pyrithiobac derivatives

Ren-Jun Wu [a, 1], Kai-Xuan Zhou [b, c, 1], Haijin Yang [d, e, 1], Guo-Qing Song [a], Yong-Hong Li [a], Jia-Xin Fu [a], Xiao Zhang [a], Shu-Jing Yu [a], Li-Zhong Wang [a], Li-Xia Xiong [a], Cong-Wei Niu [a], Fu-Hang Song [d, **], Haitao Yang [c, ***], Jian-Guo Wang [a, *]

[a] State-Key Laboratory and Research Institute of Elemento-Organic Chemistry, National Pesticide Engineering Research Center (Tianjin), College of Chemistry, Nankai University, Tianjin, 300071, China
[b] State Key Laboratory of Medicinal Chemical Biology, Nankai University, Tianjin, 300071, China
[c] Tianjin International Joint Academy of Biotechnology and Medicine, Tianjin, 300457, China
[d] State Key Laboratory of Microbial Resources, CAS Key Laboratory of Pathogenic Microbiology and Immunology, Institute of Microbiology, Chinese Academy of Sciences, Beijing, 100101, China
[e] School of Ocean Sciences, China University of Geosciences, Beijing, 100083, China

ARTICLE INFO

Article history:
Received 6 December 2018
Received in revised form
18 January 2019
Accepted 1 February 2019
Available online 14 February 2019

Keywords:
Pyrithiobac derivative
Acetohydroxyacid synthase
SARS-CoV M^{pro}
Crystal structure
Biological activity

ABSTRACT

Since pyrithiobac (PTB) is a successful commercial herbicide with very low toxicity against mammals, it is worth exploring its derivatives for an extensive study. Herein, a total of 35 novel compounds were chemically synthesized and single crystal of **6**–**6** was obtained to confirm the molecular structure of this family of compounds. The novel PTB derivatives were fully evaluated against various biological platforms. From the bioassay results, the best AHAS inhibitor **6**–**22** displayed weaker herbicidal activity but stronger anti-*Candida* activity than PTB did. For plant pathogenic fungi, **6**–**26** showed excellent activity at 50 mg/L dosage. Preliminary insecticidal activity and antiviral activity were also observed for some title compounds. Strikingly, **6**–**5** exhibited a promising inhibitory activity against SARS-CoV M^{pro} with IC_{50} of 4.471 μM and a low cellular cytotoxicity against mammalian 293 T cells. Based on the results of molecular modeling, HOMO-1 was considered to be a factor that affects AHAS inhibition and a possible binding mode of **6**–**5** with SARS-CoV M^{pro} was predicted. This is the first time that PTB derivatives have been studied as biological agents other than herbicides. The present research hence has suggested that more attentions should be paid to compounds belonging to this family to develop novel agrochemicals or medicines.

1. Introduction

The thioether (or sulfoether) compounds are of great interest because they are either useful intermediates for organic synthesis or meaningful agents with biological activities [1]. For example, dimethyl sulfide and phenyl sulfide are common industrial chemicals for the synthesis of pesticides, medicines and dyes. Diallyl sulfide, a naturally occurring component of garlic, exhibits anticancer activity [2]. Methionine was reported in the 1950s to have therapeutic effect against infective hepatitis [3]. Song et al. synthesized a series of 1,3,4-oxadiazole thioether derivatives (example-a) and found them to display strong antibacterial activity [4]. Yang et al. prepared some novel thioether-substituted flavonoids (example-b) and some of them showed satisfactory antiproliferative activity [5]. Chu et al. designed some nucleoside conjugates of thioether phospholipids (example-c) and favorable *anti*-HIV activity was observed [6].

Pyrithiobac (PTB) is a particular thioether compound in that the sulfur atom is connected by a phenyl ring and a pyrimidine ring,

* Corresponding author.
** Corresponding author.
*** Corresponding author.
E-mail addresses: songfuhang@163.com (F.-H. Song), yanght@tju.edu.cn (H. Yang), nkwjg@nankai.edu.cn (J.-G. Wang).
[1] These three authors contributed equally to this work.

https://doi.org/10.1016/j.ejmech.2019.02.002
0223-5234/

which in fact is a powerful herbicide used in cotton fields with excellent selectivity [7]. The target of this herbicide is acetehydroxyacid synthase (AHAS, EC 2.2.1.6), a special biological enzyme that exists only in plants and microbes [8]. A recent crystallography study showed that PTB binds with plant AHAS in a similar cavity provided by two neighboring subunits [9]. Nevertheless, PTB derivatives have not been fully explored till now. As is known, compounds containing heterocycle ring such as pyrimidine or triazine often show diverse agricultural or medicinal activities. For instances, pyramat is a successful insecticide with a pyrimidine ring developed in the 1960s and anilazine is a traditional fungicide with a triazine ring that have been used for over 60 years [10,11]. Recently, some aromatic disulfides with pyrimidine ring (example-d) were discovered to be potent inhibitors of main protease of severe acute respiratory syndrome coronavirus (SARS-CoV M^{pro}) [12]. The chemical structures of dimethyl sulfide, phenyl sulfide, diallyl sulfide, methionine, example-a, example-b, example-c, pyrithiobac, pyramat, anilazine and example-d mentioned above are shown in Fig. 1.

In view of these backgrounds, herein we have designed and synthesized a series of 35 novel PTB derivatives and investigated their biological activities upon various bioassay platforms. To our delight, the title compounds exhibited multiple bioactivities, against agricultural weeds, insects, pathogenic plant fungi or plant virus, and medicinal infections caused by fungus or SARS-associated coronavirus. For compounds that showed remarkable activity against SARS-CoV M^{pro}, very low cellular cytotoxicity was observed against mammalian 293 T cells. In addition, the chemical structure of **6**–**6** was elucidated clearly from single crystal X-ray diffraction, which evidently indicated that these PTB derivatives were chemically prepared successfully. Molecular simulations were performed and it was found that HOMO-1 might contribute to AHAS inhibition from DFT calculation and a plausible binding mode of inhibitor **6**–**5** with SARS-CoV M^{pro} was generated via molecular docking.

2. Results and discussion

2.1. Synthesis of the PTB derivatives

The chemistry of intermediates **2** and **3** is illustrated in Scheme 1, and the synthetic route for the target compound **6** is presented in Scheme 2. Although **2** and **3** were commercially available, they were chemically synthesized in our laboratory. Various mercaptobenzonitriles **2** were prepared from corresponding fluorobenzonitriles **1** via a nucleophilic substitution attacked by a sulfhydryl group provided by sodium sulfide nonahydrate to give desirable outputs. **2** were further hydrolyzed under alkaline condition from mercaptobenzonitriles to mercaptobenzoic acids **3** with satisfactory yields. Some intermediates were hard to be purified and were used directly in the following reaction. According to the literature [13], hydrolysis of **2** occurs easily under the condition of 15%

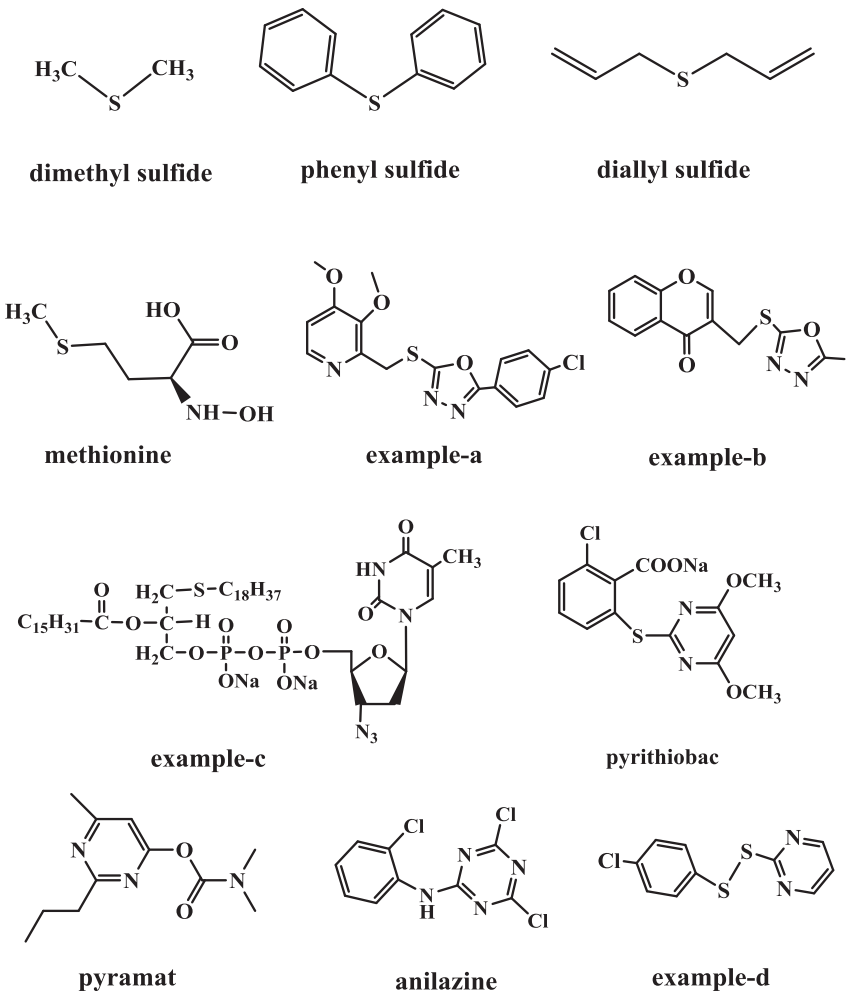

Fig. 1. Examples of industrial or bioactive thioethers and bioactive compounds containing pyrimidine or triazine ring.

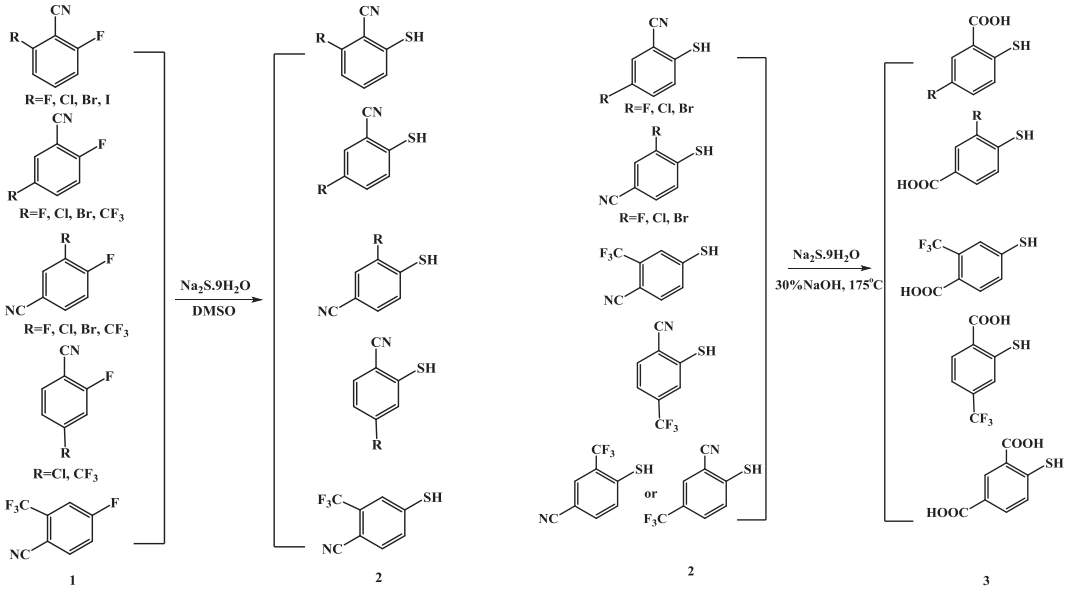

Scheme 1. General synthesis route of intermediate **2** and **3**.

sodium hydroxide at 150 °C, however, this reaction was not observed until the condition was changed to 30% sodium hydroxide at 175 °C with 0.9 equivalent of sodium sulfide nonahydrate added to the solution in an autoclave reactor. It should be noted that when there is a trifluoromethyl group in the *ortho* or *para* position of the hydrosulphonyl group of **2**, the trifluoromethyl group itself will be hydrolyzed at the same time when the cyanogroup is hydrolyzed, however when the trifluoromethyl group is at the *meta* position of the hydrosulphonyl group, the hydrolysis of trifluoromethyl group does not happen, which has been confirmed by the final compounds. This is in agreement with an early report by Jones in 1947 [14]. The synthesis and characterizations of the intermediates **2** and **3** are detailed in the supplementary material.

For the target compounds, in total there are four different synthesis routes. Compound **6**–**1** to **6**–**13** were prepared from **2** and 2-chloro-4,6-dimethoxy-1,3,5-triazine **4** using triethylamine as a base in acetonitrile [15]. Compound **6**–**14** to **6**–**21** were synthesized from **3** and **4**, but a more potent base sodium methoxide was used in methanol. Compound **6**–**34** and **6**–**35** were also started from **4**, with substituted phenyl **2′** as the nucleophile, potassium hydroxide as the base in tetrahydrofuran [16]. In all these three routes, the chlorine atom in the triazine ring is attacked and substituted by the hydrosulphonyl or hydroxyl group in **2**, **2′** and **3**. For the synthesis of compound **6**–**22** to **6**–**33**, intermediate **2** or **3** reacted with 4,6-dimethoxy-2-(methylsulfonyl)pyrimidine **5** in ethanol to give the final product, which is also a nucleophilic substitution but in this case the leaving group is a methanesulfonyl group in the pyrimidine ring and the corresponding base is sodium bicarbonate [17]. The yields for the target compounds were in the range of 10%–58%, with a majority of 20%–30%, indicating that further optimization of the reaction conditions is required.

The chemical structures of **6**–**1** to **6**–**35** were fully characterized by means of ^{1}H NMR, ^{13}C NMR and HRMS. The melting points of all the target compounds were also determined. To further confirm the molecular structure and chemical bonding of the target compounds, **6**–**6** was successfully recrystallized from ethyl acetate/petroleum ether to give colorless crystals suitable for single crystal X-ray diffraction. As shown in Fig. 2, the two aromatic rings are connected by a sulfur atom and the whole molecule adopts a bent shape, which is highly similar to the conformation of PTB in complex with plant AHAS [9].

2.2. Biological activity

2.2.1. Inhibition against fungal AHAS and Candida albicans

As can be seen in Table 1, most PTB derivatives displayed preferable inhibitory activities against *C. albicans* AHAS at 100 μM concentration, and a few of them still showed >50% inhibition at 10 μM. In contrast, PTB itself was a very weak inhibitor of this enzyme, the inhibition of which was only 40% at 100 μM. This is close to the reported data by Garcia et al. [18]. The other control ethoxysulfuron, one of the best AHAS inhibitors to date, had 96.8% inhibition even at 10 μM concentration. Among the target compounds, **6**–**1**, **6**–**3**, **6**–**5**, **6**–**9**, **6**–**14**, **6**–**17**, **6**–**18**, **6**–**22** and **6**–**27** had some antifungal activities from the YNB media cell based assay. For the anti-*Candida* activity, there is some difference between the results from RPMI 1640 media and that from YNB media, and from the latter the activity is higher. It is known that, YNB media does not contain the BCAAs while RPMI media contains these amino acids, therefore there will be a shift of the minimum inhibitory concentration (MIC) values between the data from the two medias if AHAS inhibition is the cause of the antifungal activity. The results here indicated that the observed anti-*Candida* activity was due to this reason, which is also in accordance with our previous report [19]. When the observation time changed to 48 h instead of 24 h, MIC data increased to different extent (data now shown), which means that the anti-*Candida* activity here was an inhibitory effect, not a fungicidal effect. There exists a strong correlation between the fungal AHAS inhibition data and the antifungal activity for **6**–**9**, **6**–**22** and **6**–**27**. No antifungal activity was found for any compound with very weak AHAS inhibition. For comparison, PTB did not have any inhibitory activity in the cell based assay at all the conditions, however, ethoxysulfuron was a very potent inhibitor in the YNB media, with MIC values of 0.39 mg/L against all the three fungal isolates. These experimental results were similar to the reported potencies of the two commercial AHAS inhibitors [18,19].

2.2.2. Inhibition against plant AHAS and herbicidal activity

The *in vitro* inhibition of *Arabidopsis thiliana* AHAS and herbicidal activity of the target compounds are listed in Table 2.

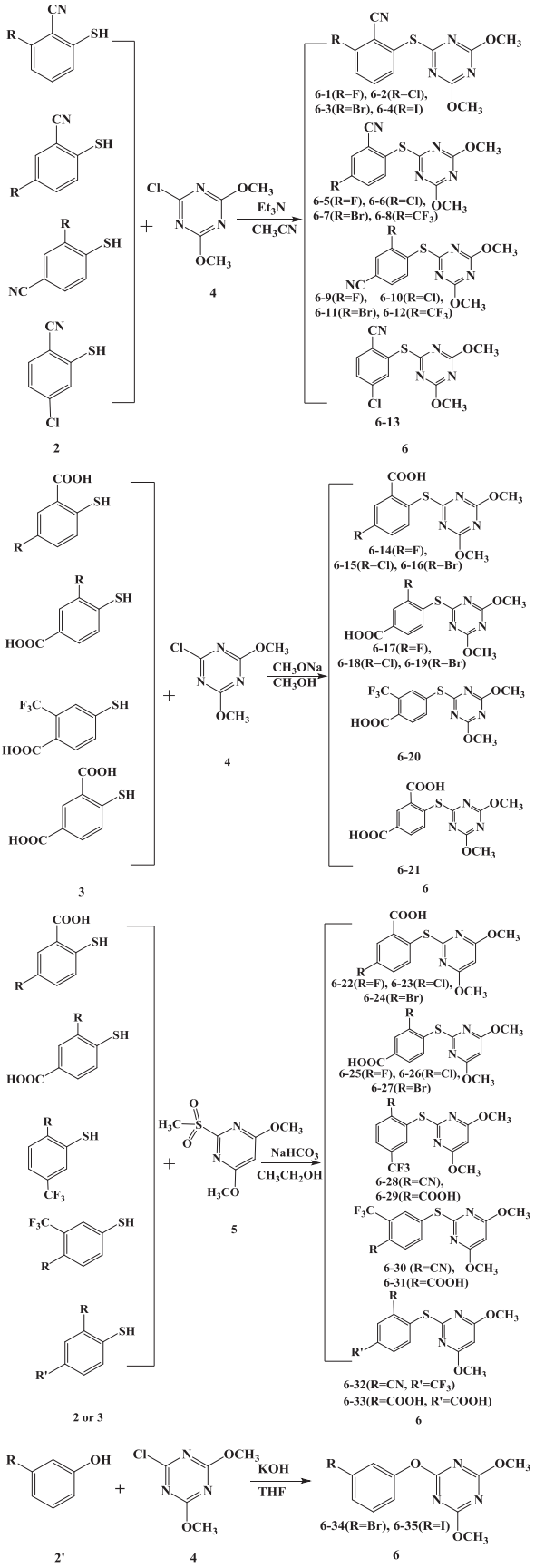

Scheme 2. Chemical synthesis route for the target compounds.

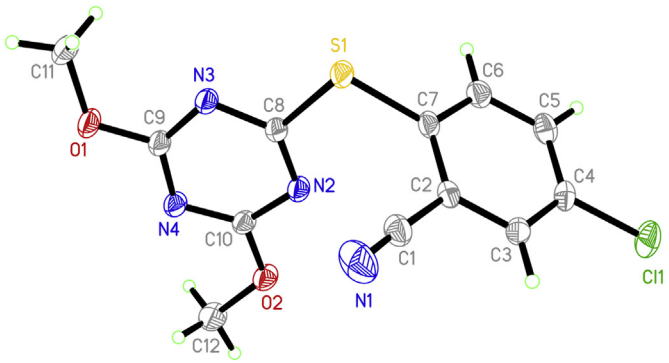

Fig. 2. Crystal structure of compound **6**–**6**.

Generally, most compounds demonstrated excellent inhibition of plant AHAS at 100 μM concentration. Compound **6**–**13**, **6**–**22**, **6**–**23**, **6**–**24**, **6**–**25**, **6**–**26** and **6**–**27** displayed complete inhibition of AHAS, as well as PTB. At 10 μM concentration, compound **6**–**21**, **6**–**22** and **6**–**24** still contributed >60% AHAS inhibition. For the *in vivo* herbicidal activity, compound **6**–**22**, **6**–**24**, **6**–**25**, **6**–**34** and **6**–**35** displayed >80% rape root growth inhibitory activity at 100 mg/L dosage, while compound **6**–**4**, **6**–**5**, **6**–**9**, **6**–**10**, **6**–**16**, **6**–**18**, **6**–**23**, **6**–**26**, **6**–**28** and **6**–**29** possessed >50% herbicidal activity. At 10 mg/L, compound **6**–**22**, **6**–**24** and **6**–**35** still maintained >70% rape root inhibition. As can be seen, PTB was not only a very strong inhibitor of plant AHAS, but also an extremely potent herbicide. Taken together the plant AHAS inhibition data and herbicidal activity, **6**–**22** and **6**–**24** were subjected to greenhouse pot assay for further evaluation, which is illustrated in Table S1. At 300 g/ha dosage, these two compounds displayed potent herbicidal activities, in both pre-emergence and post-emergence assays for dicot weed species *Brassica campestris* and *Amaranthus retroflexu*. Interestingly, **6**–**24** also showed 72.3% inhibition against monocot *Echinochloacrus-galli* from the post-emergence assay. For comparison, the herbicidal activity of PTB was much stronger even at the dosage of 30 g/ha, with the only exception of the post-emergence activity against *Echinochloacrus-galli*.

PTB is the best commercial inhibitors of plant AHAS in this family but it is a rather weak inhibitor of fungal AHAS. Meanwhile, the commercial sulfonylurea herbicide ethoxysulfuron is also a potent a strong anti-*Candida* agent. This implied that the two family of herbicidal AHAS inhibitors are different when subjected to fungal inhibition. Nevertheless, here the synthesized new derivatives demonstrated some interesting difference with PTB. For instance, **6**–**22** was more potent regarding the fungal AHAS and anti-*Candida* activity than PTB was, while the herbicidal activity of **6**–**22** was significantly weaker than that of PTB. In both fungal AHAS and plant AHAS inhibition tests, **6**–**22** was one of the best inhibitor. For **6**–**22**, there is a fluorine atom at the *para* position of the sulfur atom, while for PTB, a chlorine atom locates at the *meta* position of the sulfur atom. This minor structural difference has led to significant difference in their biological activities. A compound that combines the feature of PTB and **6**–**22** has been designed, which has fluorine atoms or chlorine atoms at both *para* and *meta* positions of the sulfur atom in the molecule. This new compound is expected to have improved AHAS inhibition.

2.2.3. Antifungal activity against plant fungi disease

Most of the target compounds together with PTB were also subjected to the bioactivity against six common plant pathogenic fungi, and the corresponding results are summarized in Table 3. The commercial fungicide chlorothalonil was used as a positive control.

Table 1
In vitro inhibitory activities fungal AHAS and their cell based activities against *C. albicans*.[a]

Compound	*C. albicans* AHAS inhibition (%)		MIC (mg/L) in RPMI 1640 media			MIC (mg/L) in YNB media		
	100 μM	10 μM	SC5314	17#	g5	SC5314	17#	g5
6–1	70.4	46.3	100	100	100	6.25	3.125	12.5
6–2	59.5	38.9	>100	>100	>100	>100	>100	>100
6–3	71.1	34.8	>100	>100	>100	12.5	6.25	12.5
6–4	69.3	45.4	>100	>100	>100	>100	>100	>100
6–5	85.1	36.4	100	100	100	50	25	50
6–6	79.9	52.1	>100	>100	>100	>100	>100	>100
6–7	81.1	37.4	>100	>100	>100	>100	>100	>100
6–8	12	0	>100	>100	>100	>100	>100	>100
6–9	85.4	55.7	100	100	100	6.25	6.25	12.5
6–10	73.6	65.4	>100	>100	>100	>100	>100	>100
6–11	68.6	32.1	>100	>100	>100	>100	>100	>100
6–12	22	10.5	>100	>100	>100	>100	>100	>100
6–13	26.3	0	>100	>100	>100	>100	>100	>100
6–14	77.6	56.1	>100	100	>100	>100	50	>100
6–15	68.8	39.3	>100	>100	>100	>100	>100	>100
6–16	96.7	59.3	>100	>100	>100	>100	>100	>100
6–17	94.9	52.3	>100	>100	>100	>100	3.125	>100
6–18	73	25.6	>100	>100	>100	100	25	100
6–19	92.4	50.1	>100	>100	>100	>100	>100	>100
6–20	21.2	8.6	>100	>100	>100	>100	>100	>100
6–21	58.7	15.6	>100	>100	>100	>100	>100	>100
6–22	97.7	73.7	100	25	100	25	3.125	25
6–23	96.6	80.6	>100	>100	>100	>100	>100	>100
6–24	97	50.5	>100	>100	>100	>100	>100	>100
6–25	91.7	81.7	>100	>100	>100	>100	>100	>100
6–26	85	62.3	>100	>100	>100	>100	>100	>100
6–27	94.6	70.7	>100	>100	>100	25	12.5	25
6–28	26.1	7.9	>100	>100	>100	>100	>100	>100
6–29	31.2	0	>100	>100	>100	>100	>100	>100
6–30	51.4	18.6	>100	>100	>100	>100	>100	>100
6–31	20.6	2.1	>100	>100	>100	>100	>100	>100
6–32	25.0	3.6	>100	>100	>100	>100	>100	>100
6–33	24	8	>100	>100	>100	>100	>100	>100
6–34	18.3	10.6	>100	>100	>100	>100	>100	>100
6–35	29.4	0	>100	>100	>100	>100	>100	>100
Pyrithiobac	40	20	>100	>100	>100	>100	>100	>100
Ethoxysulfuron	98.7	96.8	25	50	25	0.39	0.39	0.39

[a] **Measured after 24h,** 17# and g5 are two clinically isolated strains of *Candica albicans*.

At 50 mg/L concentration, the tested compounds showed moderate to excellent antifungal activity against the plant fungi. For *Sclerotinia sclerotiorum*, **6–19**, **6–20**, **6–25**, **6–26** and **6–31** exhibited >70% inhibition. For *Phytophthora capsici*, the best compound was **6–28** with inhibitory activity of 66.7%. For *Physalospora piricola*, **6–3**, **6–5**, **6–6**, **6–7** and **6–26** displayed >70% biological activity. For *Rhizoctonia cerealis*, **6–11**, **6–23**, **6–25**, **6–26**, **6–27**, **6–35** and PTB had >85% inhibitory rates, while **6–24**, **6–28** and **6–31** had >70% potency. For *Watermelon anthracnose* and *Rice bakanae*, none of the tested compounds showed powerful inhibition. The concentrations for 50% of the maximal effect (EC_{50}) of **6–11**, **6–23**, **6–25**, **6–26**, **6–27**, **6–35** and PTB against *R. cerealis* were determined subsequently and the corresponding EC_{50} data were 12.4 mg/L, 14.1 mg/L, 11.8 mg/L, 9.2 mg/L, 11.4 mg/L, 10.9 mg/L and 15.4 mg/L, respectively. The control chlorothalonil was active against all the selected fungi with inhibition data >75%, and EC_{50} against *R. cerealis* was 5.3 mg/L. Compound **6–26** was the best inhibitor among all the compounds, showing >75% inhibition against three fungi and the best inhibition of 60.6% against *R. bakanae*, which might be considered as a potential fungicide for further study. It should be pointed out that the media for this assay contains the amino acids and we failed to try these assays under YNB media, therefore antifungal activity determined here does not necessarily have direct relationship with AHAS inhibition, or AHAS inhibition might not be the sole factor. Although **6–22** was not subjected to the plant fungi assay, there were some overlaps between the anti-*Candida* activity and antifungal activities against plant fungi disease, such as **6–3**, **6–5** and **6–27**. Obviously, *C. albicans* and the plant pathogenic fungi are different species. PTB did not exhibit any anti-*Candida* activity, but it was an inhibitor of *R. cerealis*.

2.2.4. Insecticidal activity against armyworm

Table 4 presents the larvicidal activity of the target compounds against *Mythimna separata* at 600 mg/L concentration. **6–3**, **6–14** and **6–20** exhibited >75% insecticidal activity, while **6–6** and **6–9** showed no activity for this test. In contrast, the commercial pesticide rynaxypyr displayed 100% insecticidal activity at a much lower concentration of 10 mg/L, much stronger than any of the tested target compounds. This is a valuable attempt despite that these compounds possess very weak insecticidal activity, and it implies that some PTB derivatives might be useful for the research of novel insecticides.

2.2.5. Antiviral activity against tobacco mosaic virus (TMV)

Most of the title compounds were bioassayed their passivation efficacies against TMV, and the determined inhibitory values are listed in Table 5. Ten of the tested compounds, comprising **6–4**, **6–5**, **6–10**, **6–19**, **6–20**, **6–22**, **6–25**, **6–28**, **6–34** and **6–35**, were found to have *anti*-TMV activity at 500 mg/L concentration. Among these compounds, **6–20**, **6–22** and **6–25** showed >40% antiviral activity, better than that of commercial antiviral ribaviron (37.6%)

Table 2
In vitro inhibitory activities plant AHAS and their herbicidal activities.

Compound	*A. thaliana* AHAS inhibition (%)		Rape root test (%) *B. campestris*	
	100 μM	10 μM	100 mg/L	10 mg/L
6–1	86.5	34.5	26.2	2.2
6–2	79.3	19.8	17.4	0
6–3	74.7	40.3	14.3	0
6–4	66.7	51.6	51.6	0
6–5	71.2	59.2	60.3	4.6
6–6	71.3	44.9	16.6	0
6–7	85.5	57.3	14.0	0
6–8	15	11.5	8.5	0
6–9	63.3	42.9	54.2	41.8
6–10	89.6	43.2	60.3	28.4
6–11	98.3	53.1	25.0	0
6–12	10	0	5	0
6–13	100	43.6	40	34.4
6–14	68.6	3.3	33.3	1.6
6–15	59.6	5.5	24.2	0
6–16	19	12	55.1	5.2
6–17	18.7	13.8	27.6	0
6–18	15.3	12.6	58.2	0
6–19	30	22.4	34.3	0
6–20	75.5	21.8	16.5	4.0
6–21	81.7	73.3	20.3	8
6–22	100	70.1	86	72.0
6–23	100	34	54.5	0
6–24	100	61	93.6	80.7
6–25	100	40	82.2	48.0
6–26	100	31.4	73.4	30.6
6–27	100	48.9	26.4	0
6–28	91.6	18	66.1	12.3
6–29	85.5	51.8	50.0	24.6
6–30	86.2	51.2	33.5	4.7
6–31	77.4	37.7	45.2	0
6–32	72.3	28.2	25.8	0
6–33	20	5	0	0
6–34	60	6.6	87.4	32.5
6–35	84.7	8.9	88.1	80.2
Pyrithiobac	100	96	97.0	90.2

but weaker than another commercial antiviral ningnanmycin (56.4%). Therefore these compounds were subjected to further evaluation of the biological activity at 100 mg/L concentration, and the determined passivation efficacies were 6.2% for **6–20**, 11.4% for **6–22** and 6.8% for **6–25**, respectively. At this condition, ribavirin had 11.9% antiviral activity and ningnanmycin had 27.8% efficiency. These data suggests that the ningnanmycin is superior to the PTB derivatives, and **6–22** is comparable to ribaviron at the tested conditions.

2.2.6. Inhibitory activity against SARS-CoV M^{pro}

The biological activities against SARS-CoV M^{pro} of the target compounds were also evaluated in this study and the inhibitory results that were tested at 20 μM are listed in Table 6. Compound **6–4**, **6–5** and **6–7** exhibited 100% inhibition, while **6–1**, **6–2**, **6–3**, **6–6**, **6–14**, **6–17** and **6–30** displayed >75% inhibitions. At the same condition, PTB only showed 12.2% inhibition towards SARS-CoV M^{pro}. **6–4**, **6–5** and **6–7** were additionally measured their half maximal inhibitory concentration (IC_{50}) values for SARS-CoV M^{pro}, together with their half cytotoxic concentration (CC_{50}) data for 293 T cells. The determined IC_{50} for **6–4** was 3.30 μM and its CC_{50} was 30.5 μM, the corresponding data for **6–5** were 4.47 μM (IC_{50}) and >200 μM (CC_{50}), and for **6–7** were 4.54 μM (IC_{50}) and 53.5 μM (CC_{50}). Therefore **6–5** has a surprising selectivity index of 44.5, showing that it is a promising hit for further investigation. The inhibition curve of **6–5** against SARS-CoV M^{pro} is drawn in Fig. 3.

For a comparison, **6–4** and **6–5** both showed *anti*-TMV activity and inhibition against SARS-CoV M^{pro}, while other compounds are not within the overlap. There exist big difference between TMV and SARS-CoV, and it is not likely that major overlap exists between them.

Although different compounds showed different biological activities. **6–5** displayed desirable activities from all the bioassays and it has a low cellular cytotoxicity against 293 T cells. Therefore it

Table 3
Percent inhibitions against plant fungi disease at 50 mg/L dosage.

Compound	SS	PC	PP	RC	WA	RB
6–1	63.9	33.3	45.3	52.4	42.9	24.2
6–2	50.0	33.3	51.6	27.4	40.5	21.2
6–3	13.9	25.0	73.4	31.0	47.6	21.2
6–4	11.1	8.3	29.7	52.4	33.3	30.3
6–5	33.3	25.0	75.0	57.1	40.5	33.3
6–6	27.8	16.7	71.9	45.2	23.8	33.3
6–7	19.4	8.3	70.3	66.7	21.4	30.3
6–9	13.9	16.7	54.7	58.3	23.8	27.3
6–10	36.1	8.3	60.9	54.8	33.3	42.4
6–11	13.9	8.3	56.3	94.0	19.0	51.5
6–13	13.9	41.7	37.5	40.5	19.0	30.3
6–14	55.6	16.7	45.3	57.1	19.0	30.3
6–15	61.1	8.3	40.6	52.4	16.7	0.0
6–16	66.7	33.3	59.4	58.3	23.8	6.1
6–17	61.1	16.7	53.1	57.1	19.0	6.1
6–18	69.4	58.3	42.2	59.5	16.7	27.3
6–19	77.8	41.7	46.9	58.3	35.7	57.6
6–20	75.0	8.3	43.8	38.1	16.7	36.4
6–23	63.9	41.7	40.6	89.3	52.4	48.5
6–24	63.9	33.3	37.5	72.6	40.5	27.3
6–25	83.3	58.3	50.0	91.7	40.5	48.5
6–26	83.3	41.7	76.6	89.3	28.6	60.6
6–27	50.0	42.7	51.6	96.4	45.2	39.4
6–28	11.1	66.7	28.1	70.2	26.2	45.5
6–31	75.0	8.3	35.9	73.8	14.3	30.3
6–34	61.1	8.3	40.6	52.4	16.7	0.0
6–35	66.7	33.3	59.4	90.5	23.8	6.1
Pyrithiobac	64.8	44.7	60.3	86.9	45.3	12.6
Chlorothalonil	87.6	80.8	92.5	96.8	78.6	75.4

* **SS** = *S. sclerotiorum*, PC = *P. capsici*, PP = *P. piricola*, RC = *R. cerealis*, WA = *W. anthracnose*, RB = *R. bakanae*.

Table 4
Insecticidal activities against *Mythimna separata* at 600 mg/L.

Compound	Insecticidal activity (%)
6–1	20
6–2	5
6–3	75
6–4	45
6–5	20
6–6	0
6–7	20
6–9	0
6–10	30
6–11	30
6–13	25
6–14	80
6–15	40
6–16	45
6–17	30
6–18	20
6–19	10
6–20	80
6–23	5
6–24	65
6–25	30
6–26	50
6–27	50
6–28	65
Rynaxypyr[a]	100

[a] Determined at 10 mg/L dosage.

Table 5
Antiviral activities against tobacco mosaic virus.

Compound	Passivation effect (%)	
	500 mg/L	100 mg/L
6–1	0	NI[a]
6–2	0	NI
6–3	0	NI
6–4	22.8	NI
6–5	26.4	NI
6–6	0	NI
6–7	0	NI
6–9	0	NI
6–10	29.6	NI
6–11	0	NI
6–13	0	NI
6–14	0	NI
6–15	0	NI
6–16	0	NI
6–17	0	NI
6–18	0	NI
6–19	21.4	NI
6–20	42.3	6.2
6–22	47	11.4
6–23	0	NI
6–24	0	0
6–25	46.5	6.8
6–26	0	NI
6–27	0	NI
6–28	35.8	NI
6–31	0	NI
6–34	19.5	NI
6–35	17.1	NI
Ribavirin	37.6	11.9
Ningnanmycin	56.4	27.8

[a] NI = no inhibition.

Table 6
Biological activities against SARS-CoV main protease at 20 μM.

Compound	Inhibition (%)
6–1	90.8
6–2	76.6
6–3	96.3
6–4	100
6–5	100
6–6	85.1
6–7	100
6–8	0
6–9	49.7
6–10	12.8
6–11	39.3
6–12	18
6–14	94.5
6–15	24.2
6–16	48.8
6–17	89.5
6–18	25.5
6–19	25
6–20	22.2
6–21	0
6–23	4.6
6–24	0
6–25	26.8
6–26	0
6–27	0
6–28	29.9
6–29	0
6–30	85.0
6–31	21.7
6–32	0
6–33	0
6–34	0
6–35	0
pyrithiobac	12.2

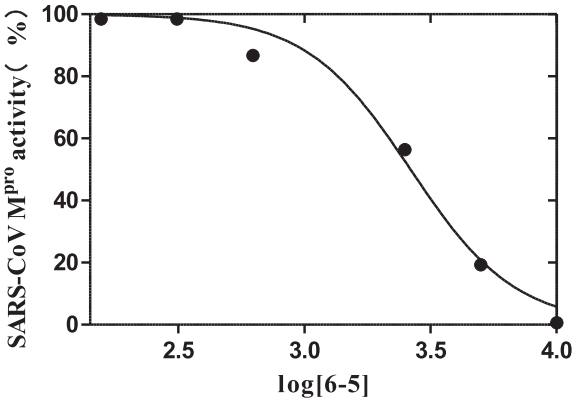

Fig. 3. Inhibition curve of compound **6–5** against SARS-CoV M^{pro} (Concentration was expressed in nM).

is an excellent starting point for further molecular design. Of course, other normal cell lines treated by **6–5** need to be accessed for better estimation of the biological safety of potent compound and this is anticipated to be done in the near future.

2.3. Molecular simulation

2.3.1. DFT calculation of typical compounds for AHAS inhibition

It is generally accepted that frontier molecular orbital contributes significantly to the inhibitor-enzyme interaction [20–23]. Among the title compounds, **6–22** showed potent inhibitions for both fungal AHAS and plant AHAS, as well as its desirable anti-*Candida* activity and herbicidal activity. Meanwhile, **6–8** and **6–12** were very weak inhibitors towards both AHASs, and no *in vivo* activities were observed. These compounds were then subjected to theoretical calculations by means of DFT/B3LYP method. From the crystal structure of PTB bound with *A. thaliana* AHAS, it is clear that the pyrimidine ring forms a π-π interaction with a neighboring residue Trp574 [9], which means that the pyrimidine ring or the triazine ring in the newly synthesized compounds might be involved in this interaction. The HOMO-1, HOMO, LUMO and LUMO+1 of these compounds were drawn Fig. 4 or Fig. S1. Comparisons of these maps revealed that here HOMO-1 might be an important factor in AHAS inhibition. For **6–22**, HOMO-1 covers not only the pyrimidine ring, but also the phenyl ring, whereas for **6–8** and **6–12**, the HOMO-1s only distribute in the heterocycle ring (Fig. 4). This suggests that **6–22** is possible to have more interactions with the enzyme than **6–8** and **6–12** do. However for HOMO, LUMO and LUMO+1 maps (seen in Fig. S1), there are either no obvious differences (HOMO and LUMO+1), or the difference is in conflict with the known π-π interaction with W574 (LUMO). Based on these thoughts, it is concluded that HOMO-1 is a non-negligible element for the further molecular design of AHAS-inhibiting PTB derivatives.

2.3.2. Molecular docking for SARS-CoV M^{pro} inhibitor

Because neither PTB nor its derivative has previously been reported to be an inhibitor of SARS-CoV M^{pro}, little is known about the binding mode. Now that we have identified that a lot of the target compounds are good inhibitors of this enzyme and **6–5** even showed very low cellular cytotoxicity, it is interesting to dock the inhibitor to the binding site to investigate the probable mode of action. FlexX is a fast, flexible docking method that uses an incremental construction algorithm to place ligands into an active site [24], which has been used previously to successfully predict the binding modes of several families of inhibitors [12,19,25]. This

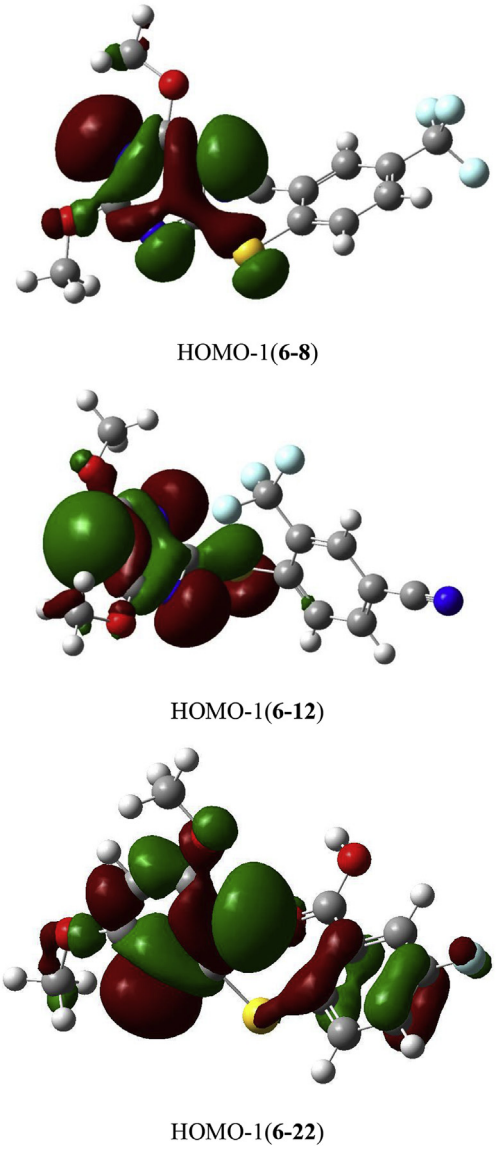

Fig. 4. HOMO-1 orbital maps for compound **6**–**8**, **6**–**12** and **6**–**22**.

program was utilized to divine the binding mode in this study. Fig. 5a is a two-dimensional illustration of the interactions between **6**–**5** and the surrounding residues of SARS-CoV M^{pro} drawn by LIGPLOT [26]. As can be seen, multiple hydrophobic interactions were formed by **6**–**5** with Thr26, Leu27, Phe140, Leu141, Gly143, His163, Glu166 and His172, while four intermolecular hydrogen bonds could be seen between **6**–**5** and Asn142, Ser144 and Cys145. Fig. 5b shows the three-dimensional molecular surface of the cavity generated by PyMOL (DeLano Scientific, South San Francisco, CA), and **6**–**5** adopted a relaxed conformation to inhabit in the cavity. The predicted binding mode has provided meaningful information for design more potent SARS-CoV M^{pro} inhibitors.

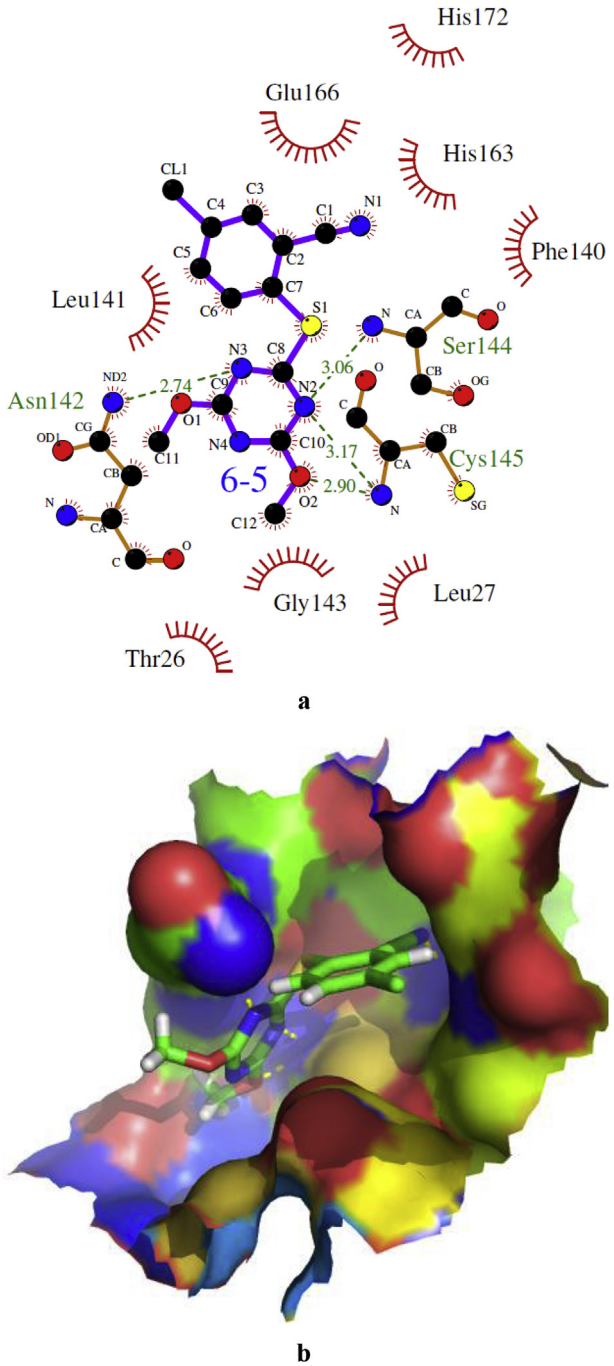

Fig. 5. Possible binding mode of compound **6**–**5** with SARS-CoV M^{pro}. (**a**) A two-dimensional representation by LIGPLOT; (**b**) Molecular surface of the binding pocket bound with the inhibitor.

3. Conclusion

Previous studies on pyrithiobac and its derivatives mostly focused on their herbicidal use. Since thioether compounds are always associated with considerable biological activities, it is necessary to investigate different bioactivities to widen their agricultural or medicinal use. As PTB itself is a highly safe compound towards mammals, compounds with similar structures are expected to have biologically safe property. In this research, a total of 35 PTB derivatives were synthesized and characterized, and this is the first time that such derivatives have been evaluated comprehensively against different bioassays. The target compounds were found to have anti-*Candida* activity, herbicidal activity, antifungal activity against plant fungi, insecticidal activity, *anti*-TMV activity and inhibitions against SARS-CoV M^{pro}. As a promising AHAS inhibitor, **6**–**22** exhibited desirable *C. albicans* inhibition and potent herbicidal activity. Interestingly, **6**–**26** displayed potent antifungal activity against plant pathogenic diseases. **6**–**22** also showed

desirable passivation efficacies against TMV. Furthermore, some compound such as **6**–**5** was identified to be potent inhibitor of SARS-CoV M^{pro}. From a DFT calculation, HOMO-1 might have impact on AHAS inhibitory activity. A feasible binding mode was constructed to explain the interaction of **6**–**5** with SARS-CoV M^{pro}. Overall, because **6**–**5** displayed activities from all the bioassays and its cell cytotoxicity data was very low, it is regarded as a lead compound for further molecular design.

4. Experimental section

4.1. General synthesis and instruments

The starting materials were procured from Bejing Ouhe, Shanghai Bide, Shanghai Energy Chemical, Qingdao Haiyang Chemical, Alfa-Aesar, Sigma-Aldrich, TCI and some local chemical suppliers. All solvents and liquid reagents were dried in advance using standard methods and distilled before use. Sodium sulfide nonahydrate was dried and stored in a drying column before use. Melting points were determined using an RT-2 melting apparatus and were uncorrected. ^{1}H NMR spectra and ^{13}C NMR were obtained using a Bruker Avance 400 MHz spectrometer. The chemical shift values (d) for the NMR spectra were reported as parts per million (ppm), using deuterated chloroform ($CDCl_3$) or dimethyl sulfoxide (DMSO-d_6) as the solvent and tetramethylsilane (TMS) as an internal reference standard. Mass spectra were recorded on an Ionspect FT-MS 7.0 T LC/mass detector instrument. Single-crystal X-ray diffraction analyses were performed on a Bruker Smart 1000 CCD diffractometer. The synthesis of intermediate **2** and **3** is depicted in Scheme 1 and the experimental data are detailed in the supplementary material. The synthesis for target PTB derivatives is shown in Scheme 2 and the experimental details are stated below.

4.2. Synthesis of the target PTB derivatives

For the synthesis of **6**–**1** to **6**–**13**, intermediate **4** (4.5 mmol) was added to the solution of intermediate **2** (3.0 mmol) in 40 mL acetonitrile under stirring, subsequently the reaction proceeded overnight at room temperature in the presence triethylamine (4.5 mmol). The mixture was then vacuumed and the remaining solid was further extracted by using a combination of ethyl acetate and water and the organic layer was kept for further process. The final product was purified by flash column chromatography using petroleum ether/ethyl acetate (80:1) and the yields were in the range of 15%–28%.

For the synthesis of **6**–**14** to **6**–**21**, intermediate **4** (2.4 mmol), intermediate **3** (1.6 mmol) and sodium methoxide (4.8 mmol) were added to 40 mL methanol. The reaction proceeded for 5 h under reflux and the mixture was then vacuumed to get rid of the solvent. The crude product was further extracted three times by using sodium hydroxide solution and ethyl acetate. The aqueous layer was then adjusted by hydrochloric acid to a pH value of 3–4. The product was extracted by ethyl acetate and finally purified by flash column chromatography using dichloromethane/methanol (80:1) and the yields were in the range of 10%–28%.

For the synthesis of **6**–**22** to **6**–**33**, intermediate **5** (4.0 mmol), intermediate **2** or **3** (2.66 mmol) and tetrabutyl ammonium bromide (0.3 mmol) were added to 50 mL 90% ethanol. After that the reaction continued for 15 h under reflux and every 2 h the pH value of the mixture was adjusted to >7 by adding saturated sodium bicarbonate solution. The crude product was further extracted three times by using sodium hydroxide solution and ethyl acetate. The aqueous layer was then adjusted by hydrochloric acid to a pH value of 3–4. The product was extracted by ethyl acetate and finally purified by flash column chromatography using dichloromethane/methanol (80:1) and the yields were in the range of 14%–35%.

For the synthesis of **6**–**34** and **6**–**35**, intermediate **4** (5.0 mmol), intermediate **2'** (5.0 mmol) and potassium hydroxide (5.0 mmol) was added to 40 mL tetrahydrofuran, after that the reaction proceeded overnight at room temperature. The mixture was then vacuumed and the remaining solid was further extracted by using a combination of ethyl acetate and water and the organic layer was kept. The final product was purified by recrystallization from ethanol and the yields were 47% and 58%.

4.2.1. 2-((4,6-Dimethoxy-1,3,5-triazin-2-yl)thio)-6-fluorobenzonitrile (**6**–**1**)

Yield 22%; m. p.: 122.8–123.4 °C; white solid; ^{1}HNMR (400 MHz, DMSO-d_6) δ 7.97–7.87 (m, 1H, ArH),7.82–7.70 (m, 2H, ArH), 3.87 (s, 6H, OCH_3); ^{13}CNMR (100 MHz, DMSO-d_6) δ 182.2, 171.5, 136.6, 136.4, 133.9, 132.4, 119.1, 118.9, 113.0, 55.6; HRMS (ESI) m/z: $[M + H]^+$ calcd for $C_{12}H_9FN_4O_2S$: 293.0503, found 293.0506.

4.2.2. 2-Chloro-6-((4,6-dimethoxy-1,3,5-triazin-2-yl)thio) benzonitrile (**6**–**2**)

Yield 25%; m. p.: 140.8–142.2 °C; white solid; ^{1}HNMR (400 MHz, DMSO-d_6) δ 7.94 (t, J = 19.2 Hz, 1H, ArH), 7.89 (d, J = 7.2 Hz, 1H, ArH), 7.85 (d, J = 7.6 Hz, 1H, ArH), 3.86 (s, 6H, OCH_3); ^{13}CNMR (100 MHz, DMSO-d_6) δ 182.0, 171.3, 137.3, 136.3, 135.4, 133.2, 132.1, 119.3, 114.9, 55.6; HRMS (ESI) m/z[M + H]$^+$ calcd for $C_{12}H_9ClN_4O_2S$: 309.0208, found 309.0201.

4.2.3. 2-Bromo-6-((4,6-dimethoxy-1,3,5-triazin-2-yl)thio) benzonitrile (**6**–**3**)

Yield 28%; m. p.: 153.3–155.4 °C; white solid; ^{1}HNMR (400 MHz, DMSO-d_6) δ 8.06 (d, J = 8.4 Hz, 1H, ArH), 7.92 (d, J = 8.0 Hz, 1H, ArH), 7.78 (t, J = 16.0 Hz,1H, ArH), 3.86 (s, 6H, OCH_3); ^{13}CNMR (100 MHz, DMSO-d_6) δ 182.1, 171.4, 137.0, 135.5, 135.2, 133.4, 126.4, 121.6, 116.3, 55.6; HRMS (ESI) m/z[M + H]$^+$ calcd for $C_{12}H_9BrN_4O_2S$: 352.9702, found 352.9709.

4.2.4. 2-((4,6-Dimethoxy-1,3,5-triazin-2-yl)thio)-6-iodobenzonitrile (**6**–**4**)

Yield 22%; m. p.: 170.4–172.8 °C; white solid; ^{1}HNMR (400 MHz, DMSO-d_6) δ 8.20 (d, J = 8.8 Hz, 1H, ArH), 7.89 (d, J = 8.0 Hz, 1H, ArH), 7.54 (t, J = 16.0 Hz, 1H, ArH), 3.87 (s, 6H, OCH_3); ^{13}CNMR (100 MHz, DMSO-d_6) δ 182.3, 171.3, 141.3, 136.8, 135.1, 132.7, 126.2, 118.6, 102.3, 55.8; HRMS (ESI) m/z[M + H]$^+$ calcd for: $C_{12}H_9IN_4O_2S$: 400.9564, found 400.9569.

4.2.5. 2-((4,6-Dimethoxy-1,3,5-triazin-2-yl)thio)-5-fluorobenzonitrile (**6**–**5**)

Yield 22%; m. p.: 128.8–130.8 °C; white solid; ^{1}HNMR (400 MHz, DMSO-d_6) δ 8.31 (s, 1H, ArH),7.92 (d, J = 8.0 Hz, 2H, ArH), 3.87 (s, 6H, OCH_3); ^{13}CNMR (100 MHz, DMSO-d_6) δ 172.2, 166.2, 139.1, 136.3, 134.5, 134.2, 129.8, 120.8, 116.4, 55.8. HRMS (ESI) m/z $[M + H]^+$ calcd for $C_{12}H_9FN_4O_2S$: 293.0503, found 293.0504.

4.2.6. 5-Chloro-2-((4,6-dimethoxy-1,3,5-triazin-2-yl)thio) benzonitrile (**6**–**6**)

Yield 20%; m. p.: 158.9–160.4 °C; white solid; ^{1}HNMR (400 MHz, DMSO-d_6) δ 8.42 (d, J = 2.0 Hz, 1H, ArH), 8.04 (dd, J = 10.4 Hz, 1H, ArH), 7.84 (d, J = 8.4 Hz, 1H, ArH), 3.87 (s, 6H, OCH_3); ^{13}CNMR (100 MHz, DMSO-d_6) δ 182.1, 171.3, 139.1, 137.5, 137.0, 130.2, 124.5, 120.8, 116.2, 55.8; HRMS (ESI) m/z $[M + H]^+$ calcd for $C_{12}H_9ClN_4O_2S$: 309.0208, found 309.0210.

4.2.7. 5-Bromo-2-((4,6-dimethoxy-1,3,5-triazin-2-yl)thio) benzonitrile (**6**–**7**)

Yield 15%; m. p.: 131.2–132.4 °C; white solid; ^{1}HNMR (400 MHz,

DMSO-d_6) δ 7.76 (d, J = 7.6 Hz, 1H, ArH), 7.54 (d, J = 7.2 Hz, 1H, ArH), 7.38 (s, 1H, ArH), 3.87 (s, 6H, OCH_3); ^{13}CNMR (100 MHz, DMSO-d_6) δ 182.5, 171.3, 139.2, 127.1, 121.8, 121.3, 121.0, 120.8, 116.8, 55.5; HRMS (ESI)m/z $[M + H]^+$ calcd for $C_{12}H_9BrN_4O_2S$: 352.9702, found 352.9698.

4.2.8. 2-((4,6-Dimethoxy-1,3,5-triazin-2-yl)thio)-5-(trifluoromethyl)benzonitrile (**6**–**8**)

Yield 20%; m. p.: 91.3–94.1 °C; white solid; ^{1}HNMR (400 MHz, $CDCl_3$) δ 8.02 (d, 1H, ArH), 7.90 (s, 1H, ArH), 7.88 (d, 1H, ArH), 3.92 (s, 3H, OCH_3); ^{13}CNMR (100 MHz, $CDCl_3$) δ 187.7, 171.3, 137.4, 135.9, 132.8, 132.5130.5, 129.6, 120.6, 115.7, 77.0, 55.5; HRMS (ESI)m/z $[M + H]^+$ calcd for $C_{13}H_9F_3N_4O_2S$: 343.0471, found 343.0473.

4.2.9. 4-((4,6-Dimethoxy-1,3,5-triazin-2-yl)thio)-3-fluorobenzonitrile (**6**–**9**)

Yield 18%; m. p.:124.4–126.4 °C; white solid; ^{1}HNMR (400 MHz, DMSO-d_6) δ 8.10 (d, J = 8.8 Hz, 1H, ArH), 7.94 (t, J = 14.4 Hz, 1H, ArH), 7.85 (d, J = 8.0 Hz, 1H, ArH), 3.85 (s, 6H, OCH_3); ^{13}CNMR (100 MHz, DMSO-d_6) δ 182.0, 171.3, 137.8, 128.3, 122.1, 119.7, 119.4, 117.0, 115.7, 55.5; HRMS (ESI) m/z $[M + H]^+$ calcd for $C_{12}H_9FN_4O_2S$: 293.0503, found:293.0508.

4.2.10. 3-Chloro-4-((4,6-dimethoxy-1,3,5-triazin-2-yl)thio) benzonitrile (**6**–**10**)

Yield 20%; m. p.: 145.3–146.4 °C; white solid; ^{1}HNMR (400 MHz, DMSO-d_6) δ 8.31 (t, J = 8.6 Hz, 1H, ArH), 8.06 (d, J = 8.0 Hz, 1H, ArH), 7.96 (d, J = 6.8 Hz, 1H, ArH), 3.85 (s, 6H, OCH_3); ^{13}CNMR (100 MHz, DMSO-d_6) δ 181.3, 170.9, 138.8, 138.4, 133.2, 132.8, 131.4, 117.0, 114.5, 55.3; HRMS (ESI) m/z $[M + H]^+$ calcd for $C_{12}H_9ClN_4O_2S$: 309.0208, found 309.0255.

4.2.11. 3-Bromo-4-((4,6-dimethoxy-1,3,5-triazin-2-yl)thio) benzonitrile (**6**–**11**)

Yield 24%; m. p.: 148.3–149.8 °C; white solid; ^{1}HNMR (400 MHz, DMSO-d_6) δ 7.73 (s, 1H, ArH), 7.53 (d, J = 8.4 Hz, 1H, ArH), 7.49 (d, J = 6.8 Hz, 1H, ArH), 3.92 (s, 6H, OCH_3); ^{13}CNMR (100 MHz, DMSO-d_6) δ 142.0, 138.0, 136.4, 135.9, 131.6, 131.0, 126.4, 120.9, 111.9, 55.5; HRMS (ESI) m/z $[M + H]^+$ calcd for $C_{12}H_9BrN_4O_2S$: 352.9702, found 352.9698.

4.2.12. 4-((4,6-Dimethoxy-1,3,5-triazin-2-yl)thio)-3-(trifluoromethyl)benzonitrile (**6**–**12**)

Yield 18%; m. p.: 146.3–149.9 °C; white solid; ^{1}HNMR (400 MHz, $CDCl_3$) δ 8.05 (d, 1H, ArH), 7.90 (s, 1H, ArH), 7.87 (d, 1H, ArH),3.88 (s, 3H, OCH_3); ^{13}CNMR (100 MHz, $CDCl_3$) δ 182.7, 171.2, 140.5, 134.6, 132.6, 130.5, 130.4, 123.5, 116.8, 114.2, 55.4; HRMS (ESI) m/z $[M + H]^+$ calcd for $C_{13}H_9F_3N_4O_2S$: 343.0471, found 343.0473.

4.2.13. 4-Chloro-2-((4,6-dimethoxy-1,3,5-triazin-2-yl)thio) benzonitrile (**6**–**13**)

Yield 25%; m. p.: 146.8–147.5 °C; white solid; ^{1}HNMR (400 MHz, DMSO-d_6) δ 7.76 (s, 1H, ArH), 7.63 (d, J = 8.0 Hz,1H, ArH), 7.56 (d, J = 8.0 Hz 1H, ArH), 3.89 (s, 6H, OCH_3); ^{13}CNMR (100 MHz, DMSO-d_6) δ 181.6, 170.3, 135.9, 134.7, 134.5, 133.3, 132.8, 132.2, 114.4, 54.5; HRMS (ESI) m/z $[M + H]^+$ calcd for $C_{12}H_9ClN_4O_2S$: 309.0208, found 309.0211.

4.2.14. 2-((4,6-Dimethoxy-1,3,5-triazin-2-yl)thio)-5-fluorobenzoic acid (**6**–**14**)

Yield 18%; m. p.: 198.4–200.3 °C; white solid; ^{1}HNMR (400 MHz, DMSO-d_6) δ 13.97 (s, 1H, COOH) 7.74 (d, J = 7.2 Hz, 2H, ArH), 7.49 (d, J = 8.4 Hz, 1H, ArH), 3.89 (s, 6H, OCH_3); ^{13}CNMR (100 MHz, DMSO-d_6) δ 173.6, 171.7, 167.2, 134.8, 129.1, 128.7, 121.1, 117.9, 167.2, 55.7; HRMS (ESI) m/z $[M + H]^+$ calcd for $C_{12}H_{10}FN_3O_4S$: 312.0449, found 312.0447.

4.2.15. 5-Chloro-2-((4,6-dimethoxy-1,3,5-triazin-2-yl)thio)benzoic acid (**6**–**15**)

Yield 10%; m. p.: 170.2–172.0 °C; white solid; ^{1}HNMR (400 MHz, DMSO-d_6) δ 12.44 (s, 1H, COOH), 7.99 (s, 1H, ArH), 7.65 (d, J = 9.6 Hz, 1H, ArH), 3.89 (s, 6H, OCH_3); ^{13}CNMR (100 MHz, DMSO-d_6) δ 169.8, 166.5, 137.6, 133.1, 130.8, 129.6, 127.1, 126.4, 123.5, 55.7; HRMS (ESI) m/z $[M + H]^+$ calcd for $C_{12}H_{10}ClN_3O_4S$: 328.0153, found: 328.0151.

4.2.16. 5-Bromo-2-((4,6-dimethoxy-1,3,5-triazin-2-yl)thio)benzoic acid (**6**–**16**)

Yield 28%; m. p.: 186.8–189.2 °C; white solid; ^{1}HNMR (400 MHz, DMSO-d_6) δ 13.62 (s, 1H, COOH), 8.04 (d, J = 9.6 Hz, 1H, ArH), 7.65 (d, J = 9.6 Hz,1H, ArH), 3.89 (s, 6H, OCH_3); ^{13}CNMR (100 MHz, DMSO-d_6) δ 183.2, 171.2, 166.6, 139.0, 136.5, 134.8, 133.1, 127.1, 123.4, 55.6; HRMS (ESI) m/z $[M - H]^-$ calcd for $C_{12}H_{10}BrN_3O_4S$: 369.9503, found 369.9498.

4.2.17. 4-((4,6-Dimethoxy-1,3,5-triazin-2-yl)thio)-3-fluorobenzoic acid (**6**–**17**)

Yield 27%; m. p.: 177.2–179.4 °C; white solid; ^{1}HNMR (400 MHz, DMSO-d_6) δ 13.19 (s, 1H, COOH) 7.65 (s, 1H, ArH), 7.56–7.62 (m, 2H, ArH), 3.92 (s, 6H, OCH_3); ^{13}CNMR (100 MHz, DMSO-d_6) δ 173.6, 171.5, 166.1, 133.4, 131.5, 127.9, 127.4, 126.7, 116.9, 55.5; HRMS (ESI) m/z $[M + H]^+$ calcd for $C_{12}H_{10}FN_3O_4S$: 312.0449, found 312.0447.

4.2.18. 3-Chloro-4-((4,6-dimethoxy-1,3,5-triazin-2-yl)thio)benzoic acid (**6**–**18**)

Yield 28%; m. p.: 195.0–196.4 °C; white solid; ^{1}HNMR (400 MHz, DMSO-d_6) δ 13.62 (s, 1H, COOH) 8.09 (s, 1H, ArH), 7.86–8.01 (s, 2H, ArH), 3.84 (s, 6H, OCH_3); ^{13}CNMR (100 MHz, DMSO-d_6) δ 182.1, 171.3, 166.1, 138.9, 138.6, 134.6, 131.8, 130.6, 128.7, 55.7; HRMS (ESI) m/z $[M - H]^-$ calcd for $C_{12}H_{10}ClN_3O_4S$: 326.0008 found: 326.0009.

4.2.19. 3-Bromo-4-((4,6-dimethoxy-1,3,5-triazin-2-yl)thio)benzoic acid (**6**–**19**)

Yield 26%; m. p.: 252.4–252.8 °C; white solid; ^{1}HNMR (400 MHz, DMSO-d_6) δ 13.35 (s, 1H, COOH) 8.13 (s, 1H, ArH), 7.95 (d, J = 7.6 Hz, 1H,ArH), 7.58 (d, J = 7.2 Hz, 1H, ArH) 3.92 (s, 6H, OCH_3); ^{13}CNMR (400 MHz, DMSO-d_6) δ 173.2, 165.4, 149.7, 139.9, 133.4, 131.2, 129.5, 126.4, 119.9, 55.0; HRMS (ESI) m/z $[M - H]^-$ calcd for $C_{12}H_{10}BrN_3O_4S$: 369.9503, found 369.9497.

4.2.20. 4-((4,6-Dimethoxy-1,3,5-triazin-2-yl)thio)-2-(trifluoromethyl)benzoic acid (**6**–**20**)

Yield 22%; m. p.: 127.5–129.8 °C; white solid; ^{1}HNMR (400 MHz, DMSO-d_6) δ 13.43 (s, 1H, COOH), 8.28 (s, 1H, ArH), 8.11 (d, J = 7.6 Hz, 1H, ArH), 7.93 (d, J = 8.0 Hz, 1H, ArH), 3.85 (s, 6H, OCH_3); ^{13}CNMR (400 MHz, DMSO-d_6) δ 182.7, 172.4, 165.6, 137.1, 135.5, 132.6, 132.4, 131.0, 129.2, 55.6; HRMS (ESI) m/z $[M + H]^+$ calcd for $C_{14}H_{12}F_3N_2O_4S$: 362.0417, found 362.0414.

4.2.21. 4-((4,6-Dimethoxypyrimidin-2-yl)thio)isophthalic acid (**6**–**21**)

Yield 26%; m. p.: 121.4–123.9 °C; yellow solid; ^{1}HNMR (400 MHz, DMSO-d_6) δ 13.40 (s, 1H, ArH), 8.38 (s, J = 7.6 Hz, 1H, ArH), 8.09 (s, 1H, ArH), 7.97 (s, 1H, ArH), 6.03 (s, 1H, ArH), 3.75 (s, 6H, OCH_3); ^{13}CNMR (100 MHz, DMSO-d_6) δ 171.4, 167.6, 166.7, 136.6, 136.6, 136.1, 132.8, 131.1, 128.7, 118.0, 87.0, 54.7; HRMS (ESI) m/z $[M + H]^+$ calcd for $C_{14}H_{12}F_3N_2O_4S$: 338.0441, found 338.0442.

4.2.22. 2-((4,6-Dimethoxypyrimidin-2-yl)thio)-5-fluorobenzoic acid (**6**–**22**)

Yield 18%, m. p.: 140.5–142.7 °C; white solid; ^{1}HNMR (400 MHz,

DMSO-d_6) δ 13.43 (s, 1H, COOH), 7.83 (d, J = 7.0 Hz, 1H, ArH), 7.65 (d, J = 8.8 Hz, 1H, ArH), 7.47 (s, 1H, ArH), 3.71 (s, 6H, OCH_3); ^{13}CNMR (100 MHz, DMSO-d_6) δ 170.0, 168.4, 168.0, 138.4, 124.5, 118.5, 118.2, 117.5, 117.3, 85.8, 53.3; HRMS (ESI) m/z $[M + H]^+$ calcd for $C_{13}H_{11}FN_2O_4S$: 311.0496, found 311.0497.

*4.2.23. 5-Chloro-2-((4,6-dimethoxypyrimidin-2-yl)thio)benzoic acid (**6**–**23**)*

Yield 14%; m. p.: 170.2–172.4 °C; white solid; ^{1}HNMR (400 MHz, DMSO-d_6) δ 13.61 (s, 1H, COOH), 8.08 (s, 1H, ArH), 7.89–7.96 (m, 2H, ArH), 6.04 (s, 1H, ArH), 3.70 (s, 6H, OCH_3); ^{13}CNMR (100 MHz, DMSO-d_6) δ 171.4, 166.2, 140.1, 138.6, 138.2, 133.9, 133.8, 130.5, 128.6, 87.0, 54.7; HRMS (ESI) m/z $[M - H]^-$ calcd for $C_{13}H_{11}ClN_2O_4S$: 325.0055, found 325.0060.

*4.2.24. 5-Bromo-2-((4,6-dimethoxypyrimidin-2-yl)thio)benzoic acid (**6**–**24**)*

Yield 21%; m. p.: 182.4–185.6 °C; white solid; ^{1}HNMR (400 MHz, DMSO-d_6) δ 13.43 (s, 1H, COOH), 7.99 (s, 1H, ArH), 7.79 (d, J = 8.4 Hz, 1H, ArH), 7.72 (d, J = 8.4 Hz, 1H, ArH), 5.98 (s, 1H, ArH), 3.74 (s, 6H, OCH_3); ^{13}CNMR (100 MHz, DMSO-d_6) δ 171.1, 169.2, 166.9, 138.5, 137.9, 134.5, 132.7, 129.3, 122.5, 86.7, 54.6; HRMS (ESI) m/z $[M - H]^-$ calcd for $C_{13}H_{11}BrN_2O_4S$: 368.9550, found: 368.9543.

*4.2.25. 4-((4,6-Dimethoxypyrimidin-2-yl)thio)-3-fluorobenzoic acid (**6**–**25**)*

Yield 27%; m. p.: 187.6–189.2 °C; white solid; ^{1}HNMR (400 MHz, DMSO-d_6) δ 13.68 (s, 1H, COOH), 7.83 (s, 2H, ArH), 7.79 (s, 1H, ArH), 6.02 (s, 1H, ArH) 3.70 (s, 6H, OCH_3); ^{13}CNMR (100 MHz, DMSO-d_6) δ 171.3, 167.8, 166.6, 137.6, 125.9, 121.5, 120.7, 116.6, 116.4, 86.6, 54.6; HRMS (ESI) m/z $[M + H]^+$ calcd for $C_{13}H_{11}FN_2O_4S$: 311.0496, found 311.0502.

*4.2.26. 3-Chloro-4-((4,6-dimethoxypyrimidin-2-yl)thio)benzoic acid (**6**–**26**)*

Yield 31%; m. p.: 179.6–180.2 °C; white solid; ^{1}HNMR (400 MHz, DMSO-d_6) δ 13.80 (s, 1H, COOH), 8.08 (s, 1H, ArH), 7.87–8.03 (2H, ArH), 6.02 (s, 1H, ArH) 3.70 (s, 6H, OCH_3); ^{13}CNMR (100 MHz, DMSO-d_6) δ 171.3, 168.1, 166.5, 154.8, 138.6, 138.0, 133.1, 130.5, 128.6, 86.7, 54.6; HRMS (ESI) m/z $[M - H]^-$ calcd for $C_{13}H_{11}ClN_2O_4S$: 325.0055, found 325.0062.

*4.2.27. 3-Bromo-4-((4,6-dimethoxypyrimidin-2-yl)thio)benzoic acid (**6**–**27**)*

Yield 24%; m. p.: 172.8–174.6 °C; white solid; ^{1}HNMR (400 MHz, DMSO-d_6) δ 13.45 (s, 1H, COOH), 8.23 (s, 1H, ArH), 7.92–8.01 (2H, ArH), 6.03 (s, 1H, ArH), 3.70 (s, 6H, OCH_3); ^{13}CNMR (100 MHz, DMSO-d_6) δ 170.8, 167.5, 165.5, 137.5, 135.4, 133.2, 130.0, 129.6, 128.6, 86.2, 54.1; HRMS (ESI)m/z [$M - H]^-$ calcd for $C_{13}H_{11}BrN_2O_4S$: 368.9550, found 368.9549.

*4.2.28. 2-((4,6-Dimethoxypyrimidin-2-yl)thio)-4-(trifluoromethyl) benzonitrile (**6**–**28**)*

Yield 28%; m. p.: 105.5–107.6 °C; white solid; ^{1}HNMR (400 MHz, DMSO-d_6) δ 8.12 (s, 1H, ArH), 7.88 (d, J = 8.0 Hz,1H, ArH), 7.56 (d, J = 8.0 Hz, 1H, ArH), 3.89 (s, 6H, OCH_3); ^{13}CNMR (100 MHz, DMSO-d_6) δ 172.8, 171.0, 167.1, 135.7, 133.8, 128.9, 126.1, 122.8, 121.4, 116.1, 87.5, 54.1; HRMS (ESI) m/z $[M + H]^+$calcd for $C_{14}H_{10}F_3N_3O_2S$: 342.0519, found 342.0524.

*4.2.29. 2-((4,6-Dimethoxypyrimidin-2-yl)thio)-4-(trifluoromethyl) benzoic acid (**6**–**29**)*

Yield 24%; m. p.: 127.4–129.3 °C; yellow solid; ^{1}H NMR (400 MHz, DMSO-d_6) δ 13.71 (s, 1H, COOH), 8.28–8.12 (m, 1H,ArH), 8.03 (d, J = 8.3 Hz, 1H, ArH), 7.89 (d, J = 8.1 Hz, 1H, ArH), 7.74 (d, J = 8.1 Hz, 1H, ArH), 6.07 (d, J = 40.3 Hz, 1H, Het-H), 3.73 (s, 6H, OCH_3); ^{13}CNMR (100 MHz, DMSO-d_6) δ 171.1, 168.7, 167.4, 139.7, 133.0, 132.6, 131.4, 131.0, 125.9, 123.2, 87.1, 54.5; HRMS (ESI) m/z $[M + H]^+$ calcd for $C_{14}H_{12}F_3N_2O_4S$: 361.0464, found 361.0469.

*4.2.30. 4-((4,6-Dimethoxypyrimidin-2-yl)thio)-2-(trifluoromethyl) benzonitrile (**6**–**30**)*

Yield 17%; m. p.: 83.3–85.4 °C; yellow solid; ^{1}HNMR (400 MHz, DMSO-d_6) δ 8.07 (s, 1H, ArH), 7.83 (d, J = 8.0 Hz 1H, ArH), 7.71 (d, J = 8.0 Hz 1H, ArH), 5.73 (s, 1H, ArH), 3.67 (s, 6H, OCH_3), ^{13}CNMR (100 MHz, DMSO-d_6) δ 171.1, 167.3, 166.6, 148.4, 137.1, 135.5, 133.8, 132.2, 131.9, 131.3, 86.7, 53.4; HRMS (ESI) m/z $[M + H]^+$ calcd for $C_{14}H_{10}F_3N_3O_2S$: 342.0519, found 342.0522.

*4.2.31. 4-((4,6-Dimethoxypyrimidin-2-yl)thio)-2-(trifluoromethyl) benzoic acid (**6**–**31**)*

Yield 35%; m. p.: 131.4–132.9 °C; yellow solid; ^{1}HNMR (400 MHz, DMSO-d_6) δ 13.65 (s, 1H, COOH), 8.14 (s, 1H, ArH), 8.01 (d, J = 7.6 Hz, 1H, ArH), 7.91 (d, J = 8.4 Hz, 1H, ArH), 6.05 (s, 1H, ArH), 3.74 (s, 6H, OCH_3); ^{13}CNMR (100 MHz, DMSO-d_6) δ 193.6, 171.3, 168.4, 167.9, 138.4, 132.7, 131.6, 130.8, 130.5, 124.9, 86.9, 54.6; HRMS (ESI) m/z $[M + H]^+$ calcd for $C_{14}H_{12}F_3N_2O_4S$: 361.0464, found 361.0463.

*4.2.32. 2-((4,6-Dimethoxypyrimidin-2-yl)thio)-5-(trifluoromethyl) benzonitrile (**6**–**32**)*

Yield 21%; m. p.: 85.6–87.4 °C; yellow solid; ^{1}HNMR (400 MHz, DMSO-d_6) δ 8.31 (s, 1H, ArH), 8.06 (d, J = 7.6 Hz, 1H, ArH), 8.00 (d, J = 7.6 Hz, 1H, ArH), 5.68 (s, 1H, ArH), 3.90 (s, 6H, OCH_3); ^{13}CNMR (400 MHz, DMSO-d_6) δ 172.7, 171.0, 164.4, 139.7, 137.4, 134.9, 128.8, 125.1, 124.7, 121.4, 83.2, 54.1; HRMS (ESI) m/z $[M + H]^+$ calcd for $C_{14}H_{10}F_3N_3O_2S$: 342.0519, found 342.0521.

*4.2.33. 4-((4,6-Dimethoxypyrimidin-2-yl)thio)isophthalic acid (**6**–**33**)*

Yield 26%; m. p.: 121.4–123.9 °C; yellow solid; ^{1}HNMR (400 MHz, DMSO-d_6) δ 13.40 (s, 1H, ArH), 8.38 (s, J = 7.6 Hz, 1H, ArH), 8.09 (s, 1H, ArH), 7.97 (s, 1H, ArH), 6.03 (s, 1H, ArH), 3.75 (s, 6H, OCH_3); ^{13}CNMR (100 MHz, DMSO-d_6) δ 171.4, 167.6, 166.7, 136.6, 136.6, 136.1, 132.8, 131.1, 128.7, 118.0, 87.0, 54.7; HRMS (ESI) m/z $[M + H]^+$ calcd for $C_{14}H_{12}F_3N_2O_4S$: 337.0489, found 337.0490.

*4.2.34. 2-(3-bromophenoxy)-4,6-dimethoxy-1,3,5-triazine (**6**–**34**)*

Yield 47%; m. p.: 83.5–85.2 °C; white solid; ^{1}HNMR (400 MHz, $CDCl_3$) δ 7.63 (s, 1H), 7.31 (s, 1H), 7.24 (s, 1H), 3.81 (s, 7H); ^{13}CNMR (100 MHz, DMSO-d_6) 155.6, 129.7, 128.3, 124.1, 122.8, 121.7, 117.8, 113.3, 55.5; HRMS (ESI) m/z $[M + H]^+$ calcd for $C_{11}H_{10}BrN_3O_3$: 311.9978, found: 311.9984.

*4.2.35. 2-(3-iodophenoxy)-4,6-dimethoxy-1,3,5-triazine (**6**–**35**)*

Yield 58%; m. p.: 80.2–81.4 °C; white solid; ^{1}HNMR (400 MHz, DMSO-d_6) δ 7.63–7.73 (m, 2H, ArH), 7.23–7.31 (m, 2H, ArH), 3.91 (s, 6H, OCH_3); ^{13}CNMR (100 MHz, DMSO-d_6) δ 173.7, 173.0, 152.4, 135.2, 131.8, 130.8, 121.8, 94.8, 55.8; HRMS (ESI) m/z $[M + H]^+$ calcd for $C_{11}H_{10}BrN_3O_3$:359.9840, found 359.9833.

4.3. Evaluation of biological activities

4.3.1. Fungal AHAS inhibition and plant AHAS inhibition

The *C. albican* AHAS catalytic subunit and *A. thaliana* AHAS catalytic subunit were expressed and purified as describe previously [19,27]. AHAS activity was measured using the colorimetric assay in 50 mM potassium phosphate (pH 7.0) containing 50 mM pyruvate, 1 mM thiamine diphosphate, 10 mM $MgCl_2$, and 10 μM FAD. After incubation for 30 min at 37 °C (for fungal AHAS at 30 °C),

acetolactate was estimated [28].

4.3.2. Antifungal activity against C. albicans

The *Candica albicans* strains used in this study include standard strain SC5314, two clinical isolates g5 and 17# and the recipe and procedure for the measurement of antifungal activity is similar with the published method [19,29]. Yeast nitrogen base (YNB) medium and RPMI 1640 medium were both used for the determination whether AHAS is a probable cause of the antifungal data. The microdilution plates were incubated at 35 °C over a period of 72 h and visual readings of the cultures were taken at 24 h. MICs were defined as the lowest concentrations of the compounds that can inhibit visible fungal growth.

4.3.3. Herbicidal activity

The rape (*Brassica campestris* L.) root growth inhibition assay was detailed before [27]. Rape seeds were soaked in distilled water for 4 h before they were placed on a filter paper in a 6-cm Petri plate, to which 2 mL of inhibitor solution had been added in advance. Usually, 15 seeds were used on each plate. The plate was placed in a dark room and allowed to germinate for 48 h at 28 °C. The lengths of 10 rape roots selected from each plate were measured and the means were calculated.

The pre-emergence and post-emergence greenhouse pot herbicidal activities were evaluated against monocotyledonous weeds (*Echinochloacrus-galli* and *Digitaria adscendens*) and dicotyledonous weeds (*Brassica campestris* and *Amaranthus retroflexus*) using methods reported previously [30].

4.3.4. Antifungal activities against plant pathogenic fungus

The fungicidal activities of the target compounds were tested against *S. sclerotiorum*, *P. capsici*, *P. piricola*, *R. cerealis*, *W. anthracnose* and *R. bakanae*, the method of which was described previously [31]. The relative inhibitory ratio (%) was determined by the mycelium growth rate method at 50 mg/L concentration. Chlorothalonil and PTB were used as controls. The EC_{50} values of selected compounds against *R. cerealis* were calculated by equation (1) [27].

$$\text{Probit} = m(\log_{10}[I]\text{-}\log_{10}[EC_{50}])+5 \quad (1)$$

4.3.5. Larvicidal activity against Mythimna separata

The insecticidal activity of title compounds and rynaxypyr against oriental armyworm (*Mythimna separata)* was tested according to the leaf-dip method using the reported procedure at 600 mg/L dose [32].

4.3.6. Passivation efficacies against TMV

TMV was inhibited by mixing with the compound solution at the same volume for 30 min. The mixture was then inoculated on the left side of the leaves of *N. tabacum L.*, whereas the right side of the leaves was inoculated with the mixture of solvent and the virus for control. The local lesion numbers were recorded 3–4 days after inoculation, as reported previously [33]. The inactivation effect was evaluated at 500 mg/L or 100 mg/L.

4.3.7. SARS-CoV M^{pro} inhibition assay

SARS-CoV M^{pro} was expressed and purified previously [34], and the inhibition assay was detailed before by us [12]. Briefly, the assays were conducted by fluorescence resonance energy transfer. The settled concentrations of proteins, compounds and substrate were preheated at 37 °C and oscillated. The excitation/emission light was 320/405 nm, and the test was carried out every 5 s for 200 times. IC_{50} values for selected compounds were calculated by equation (2).

$$V_0/V = 1+[I]/IC_{50} \quad (2)$$

4.3.8. Cytotoxicity assay for the determination of CC_{50}

MTT assay was employed to test the cytotoxic effect of selected compounds, which is similar to a published procedure [35]. 293 T Cells in logarithmic phase were collected and moved to 96-microwell plates (12000 cells/well) overnight. After treatment of 48 h with various concentrations of compounds, 15 μL MTT dye was added to each well, followed by incubating for an additional 4 h. The suspension was discarded and 100 μL DMSO was added to each well, after that OD_{570} was read. CC_{50} value was defined as the concentration of the compound reducing cell viabilityby 50%.

4.4. In silico molecular modeling

Sybyl 7.3 (Tripos Inc., St Louis, MO) was used to construct the chemical structures for the molecular simulations. The crystal structure of **6**–**6** was regarded as the starting conformation of the investigated compounds. The molecules were assigned Gasteiger-Hückel charges and minimized by the Tripos force field when convergence reached 0.001 kcal/mol/Å.

4.4.1. DFT calculation

Representative compounds **6**–**6**, **6**–**12** and **6**–**22** were chosen for DFT geometry optimization by the SCF method using the B3LYP function with a basis set of 6-31G(d, p) to describe their molecular properties. Gaussian03 was used to perform the calculations [36]. The optimized molecular structures by Sybyl were used as the initial conformations. All computations were conducted for the ground states of these molecules as singlet states. All of the convergent precisions used were the system's default values.

4.4.2. Molecular docking using FlexX

The crystal structure of SARS-CoV M^{pro} in complex with inhibitor (pdb code 2AMD) was retrieved from the protein databank. All water molecules were removed, and hydrogen atoms were added in the standard geometry. Any amino acid residue within 6.5 Å of the location of the original inhibitor was considered to be in the binding pocket. Cscore calculation was enabled and set to serial mode.

Acknowledgment

This work was financially supported by the Natural Science Foundation of China (No.21672114). This work was also dedicated to the 100th anniversary of Nankai University.

Appendix A. Supplementary data

Supplementary data to this article can be found online at https://doi.org/10.1016/j.ejmech.2019.02.002.

References

[1] P. Devendar, G.F. Yang, Sulfur-containing agrochemicals, Top. Curr. Chem. (Cham). 375 (2017) 82.
[2] J.F. Brady, D.C. Li, H. Ishizaki, C.S. Yang, Effect of diallyl sulfide on rat liver microsomal nitrosamine metabolism and other monooxygenase activities, Cancer Res. 48 (1988) 5937–5940.
[3] J. Strom, Methionine in the treatment of acute hepatitis, Br. Med. J. 1 (1950) 1168–1169.

[4] X. Song, P. Li, M. Li, A. Yang, L. Yu, L. Luo, D. Hu, B. Song, Synthesis and investigation of the antibacterial activity and action mechanism of 1,3,4-oxadiazole thioether derivatives, Pestic. Biochem. Physiol. 147 (2018) 11–19.
[5] W. Huang, Q. Chen, W.C. Yang, G.F. Yang, Efficient synthesis and anti-proliferative activity of novel thioether-substituted flavonoids, Eur. J. Med. Chem. 66 (2013) 161–170.
[6] C.I. Hong, A. Nechaev, A.J. Kirisits, R. Vig, C.R. West, K.K. Manouilov, C.K. Chu, Nucleoside conjugates. 15. Synthesis and biological activity of anti-HIV nucleoside conjugates of ether and thioether phospholipids, J. Med. Chem. 39 (1996) 1771–1777.
[7] Y. Nezu, Y. Saito, S. Takahashi, Y. Tomoda, Development of a new cotton herbicide, pyrithiobac sodium, J. Pestic. Sci. 24 (1999) 217–229.
[8] R.G. Duggleby, S.S. Pang, Acetohydroxyacid synthase, J. Biochem. Mol. Biol. 33 (2000) 1–36.
[9] M.D. Garcia, A. Nouwens, T.G. Lonhienne, L.W. Guddat, Comprehensive understanding of acetohydroxyacid synthase inhibition by different herbicide families, Proc. Natl. Acad. Sci. U.S.A. 114 (2017) E1091–E1100.
[10] M.H. Weiden, Toxicity of carbamates to insects, Bull. World Health Organ. 44 (1971) 203–213.
[11] J.F. Lawrence, L.G. Panopio, Comparison of gas and liquid chromatography for determination of anilazine in potatoes and tomatoes, J. Assoc. Off. Anal. Chem. 63 (1980) 1300–1303.
[12] L. Wang, B.B. Bao, G.Q. Song, C. Chen, X.M. Zhang, W. Lu, Z. Wang, Y. Cai, S. Li, S. Fu, F.H. Song, H. Yang, J.G. Wang, Discovery of unsymmetrical aromatic disulfides as novel inhibitors of SARS-CoV main protease: chemical synthesis, biological evaluation, molecular docking and 3D-QSAR study, Eur. J. Med. Chem. 137 (2017) 450–461.
[13] M. F. Chen, Preparation Method of 6-Chloro-2-Mercaptobenzoic Acid, Chinese Invention Patent, ZL 201310321702.vol 5.
[14] R.G. Jones, Ortho and para substituted derivatives of benzotrifluoride, J. Am. Chem. Soc. 69 (1947) 2346–2350.
[15] I. Sosic, B. Stefane, A. Kovac, S. Turk, D. Blanot, S. Gobec, The synthesis of novle 2,4,6-trisubstituted 1,3,5-triazines: a search for potential MurF enzyme inhibitors, Heterocycles 81 (2010) 91–115.
[16] X.-J. Li, J.-L. Zhang, Y. Geng, Z. Jin, Nickel-catalyzed Suzuki-Miyaura coupling of heteroaryl ethers with arylboronic acids, J. Org. Chem. 78 (2013) 5078–5084.
[17] S. Ravi, K.M. Mathew, D. Padmanabhan, V.K.P. Unny, N. Sivaprasad, A facile synthesis of [14C] pyrithiobac sodium, J. Labelled Comp. Rad. 49 (2006) 339–343.
[18] M.D. Garcia, S.M.H. Chua, Y.S. Low, Y.T. Lee, K. Agnew-Francis, J.G. Wang, A. Nouwens, T. Lonhienne, C.M. Williams, J.A. Fraser, L.W. Guddat, Commercial AHAS-inhibiting herbicides are promising drug leads for the treatment of human fungal pathogenic infections, Proc. Natl. Acad. Sci. U.S.A. 115 (2018) E9649–E9658.
[19] R.J. Wu, T. Ren, J.Y. Gao, L. Wang, Q. Yu, Z. Yao, G.Q. Song, W.B. Ruan, C.W. Niu, F.H. Song, L.X. Zhang, M. Li, J.G. Wang, Chemical preparation, biological evaluation and 3D-QSAR of ethoxysulfuron derivatives as novel antifungal agents targeting acetohydroxyacid synthase, Eur. J. Med. Chem. 162 (2019) 348–363.
[20] J. Wang, H. Tan, Y. Li, Y. Ma, Z. Li, L.W. Guddat, Chemical synthesis, in vitro acetohydroxyacid synthase (AHAS) inhibition, herbicidal activity, and computational studies of isatin derivatives, J. Agric. Food Chem. 59 (2011) 9892–9900.
[21] B.L. Wang, Y.X. Shi, S.J. Zhang, Y. Ma, H.X. Wang, L.Y. Zhang, W. Wei, X.H. Liu, Y.H. Li, Z.M. Li, B.J. Li, Syntheses, Biological activities and SAR studies of novel carboxamide compounds containing piperazine and arylsulfonyl moieties, Eur. J. Med. Chem. 117 (2016) 167–178.
[22] X. Huang, T. Liu, J. Gu, X. Luo, R. Ji, Y. Cao, H. Xue, J.T. Wong, B.L. Wong, G. Pei, H. Jiang, H. Chen, 3D-QSAR model of flavonoids binding at benzodiazepine site in GABAA receptors, J. Med. Chem. 44 (2001) 1883–1891.
[23] Y. Ma, J.G. Wang, B. Wang, Z.M. Li, Integrating molecular docking, DFT and CoMFA/CoMSIA approaches for a series of naphthoquinone fused cyclic α-aminophosphonates that act as novel topoisomerase II inhibitors, J. Mol. Model. 17 (2011) 1899–1909.
[24] M. Rarey, B. Kramer, T. Lengauer, G. Klebe, A fast flexible docking method using an incremental construction algorithm, J. Mol. Biol. 261 (1996) 470–489.
[25] J. Shang, W.M. Wang, Y.H. Li, H.B. Song, Z.M. Li, J.G. Wang, Synthesis, crystal structure, in vitro acetohydroxyacid synthase inhibition, in vivo herbicidal activity, and 3D-QSAR of new asymmetric aryl disulfides, J. Agric. Food Chem. 60 (2012) 8286–8293.
[26] A.C. Wallace, R.A. Laskowski, J.M. Thornton, LIGPLOT: a program to generate schematic diagrams of protein-ligand interactions, Protein Eng. 8 (1995) 127–134.
[27] J.G. Wang, Z.M. Li, N. Ma, B.L. Wang, L. Jiang, S.S. Pang, Y.T. Lee, L.W. Guddat, R.G. Duggleby, Structure-activity relationships for a new family of sulfonylurea herbicides, J. Comput. Aided Mol. Des. 19 (2005) 801–820.
[28] B.K. Singh, M.A. Stidham, D.L. Shaner, Assay of acetohydroxyacid synthase, Anal. Biochem. 171 (1988) 173–179.
[29] Clinical and Laboratory Standards Institute (CLSI), Reference Method for Broth Dilution Antifungal Susceptibility Testing of Yeasts; Approved Standard, third ed., CLSI, Wayne, PA, 2008. Document M27-A3.
[30] H. Xu, X.H. Hu, X.M. Zou, B. Liu, Y.Q. Zhu, Y. Wang, F.Z. Hu, H.Z. Yang, J. Agric. Food Chem. 56 (2008) 6567–6572.
[31] W. Wei, D. Cheng, J. Liu, Y. Li, Y. Ma, Y. Li, S. Yu, X. Zhang, Z. Li, Design, synthesis and SAR study of novel sulfonylureas containing an alkenyl moiety, Org. Biomol. Chem. 14 (2016) 8356–8366.
[32] J.B. Liu, Y.X. Li, X.L. Zhang, X.W. Hua, C.C. Wu, W. Wei, Y.Y. Wan, D.D. Cheng, L.X. Xiong, N. Yang, H.B. Song, Z.M. Li, Novel anthranilic diamide scaffolds containing N-substituted phenylpyrazole as potential ryanodine receptor cctivators, J. Agric. Food Chem. 64 (2016) 3697–3704.
[33] K. Wang, B. Su, Z. Wang, M. Wu, Z. Li, Y. Hu, Z. Fan, N. Mi, Q. Wang, Synthesis and antiviral activities of phenanthroindolizidine alkaloids and their derivatives, J. Agric. Food Chem. 58 (2010) 2703–2709.
[34] H. Yang, M. Yang, Y. Ding, Y. Liu, Z. Lou, Z. Zhou, L. Sun, L. Mo, S. Ye, H. Pang, G.F. Gao, K. Anand, M. Bartlam, R. Hilgenfeld, Z. Rao, The crystal structures of severe acute respiratory syndrome virus main protease and its complex with an inhibitor, Proc. Natl. Acad. Sci. U. S. A 100 (2003) 13190–13195.
[35] K. Chen, Y.L. Zhang, J. Fan, X. Ma, Y.J. Qin, H.L. Zhu, Novel nicotinoyl pyrazoline derivates bearing N-methyl indole moiety as antitumor agents: design, synthesis and evaluation, Eur. J. Med. Chem. 156 (2018) 722–737.
[36] M.J. Frisch, G.W. Trucks, H.B. Schlegel, et al., Gaussian 03, Revision C. 01, Gaussian, Inc., Wallingford CT, 2004.